Computational analysis as a tool for the study of the porosity system and the mechanical properties of fractal metal foams

L. Pérez and P. Pérez

Department of Mechanical Engineering, Advanced Center for Electrical and Electronic Engineering (Basal Project FB0008). Universidad Técnica Federico Santa María, Av. España 1680, Casilla 110-V, Valparaíso, Chile.

L. E. Carranza

Facultad de Ingeniería Mecánica, Universidad Michoacana de San Nicolás de Hidalgo, Ciudad Universitaria, 58030, Morelia, México.

M. Rivero and I. Alfonso

Instituto de Investigaciones en Materiales, Unidad Morelia, Universidad Nacional Autónoma de México, Campus Morelia UNAM. Antigua Carretera a Pátzcuaro No. 8701, 58190, Morelia, Michoacán, México. e-mail: ialfonso@unam.mx

Received 24 September 2024; accepted 28 November 2024

This work studies possible morphologies present in fractal foams with dual pore distribution, focalizing the analysis in features characterizing the pore network. These studies were conducted using foams modelled through the combined use of Discrete and Finite Element Methods (DEM and FEM, respectively). DEM was used to generate pore coordinates, for in a second step modelling pores of varied sizes using FEM. These models allowed to obtain fractal foams with morphologies closer to real experimental foams, which is essential for the subsequent estimation of their mechanical properties through FEM. Using different measurement methods, some analyzes were carried out, such as the effect of the dimension of the Representative Volume Element (RVE) on the porosity percentage, the number of nodes until a convergent behavior, the interconnectivity of the pores, the importance of the pore wall thickness and the fractal dimension determination. The effect of these parameters on the simulated mechanical properties of the foams was analyzed throw the use of FEM.

Keywords: Metal foams; fractal; discrete element method; finite element method; porosity.

DOI: https://doi.org/10.31349/RevMexFis.71.041002

1. Introduction

The study of the metallic foams has increased exponentially in the last years, motivated by their excellent combination of properties due to the relatively high strength of the metal alloys matrices and light weight derived from the porous system [1–3]. They can reach relative densities as low as 0.1 with porosities raising more than 90% [1–4]. Metal foams are mainly used in the transportation industry and for structural purposes, where various of their properties are required, such as low weight, impact and noise absorption, recyclability and corrosion resistance [4]. Much of the research about these materials is focused on their manufacturing processes and the complete characterization of their porous system, which governs possible applications. Sometimes and depending on the application, more complex porous systems are required, as the present in the hierarchical or fractal foams. This kind of multi-scaled porosity is characterized by the combination of two (dual) or more kind of pores of assorted sizes. Generated pores can be organized as open, closed, or combined cells, not only presenting different sizes but also different shapes and distributions [5–7]. Fractal porosity generally has well defined ratios between the relative quantities and sizes of small and large pores, which are quantified using the fractal dimension (D_f) [7]. This parameter can be obtained from *log (relative quantities)/log (sizes ratio)*. Different processes have been reported in literature for manufacturing fractal foams, such as additive manufacture, the infiltration on fractal removable space holder particles; or through the mixture of these particles with metal powders [7–12]. Their applications include energy conversion and storage, catalysis, photocatalysis, adsorption, separation, sensing and biomedicals [6–9], where each porosity has a different function. Due to this new trend in their research, the complete characterization of the fractal foams is essential. It includes not only the porosity percentage and the fractal dimension, but also parameters such as wall thickness, interconnection of pores and their effect on the mechanical properties. The characterization of the fractal foams needs more than one technique due to the different scales of the pores, as could be macrography or Optical and Scanning Electron Microscopies (OM and SEM, respectively). Image analysis derived from the figures obtained thought these techniques also allows the determination of more specific parameters, such as the pore wall thickness, the interpenetration, and the pores neck, which will be further defined in this work using examples. Fine characteristics such as the pixels of the image to be analyzed could influence the results obtained, including the fractal dimension (D_f) of the image, which presents a measure of the complexity of the pore system. D_f can be determined using the

box-counting method, and could be a valuable tool for analyzing the describe the pore network [7]. To conduct these characterizations, the foams must be first manufactured, with the subsequent cost of materials, energy, and time. Besides, not always the manufacturing process allows to obtain hierarchical foams, with the desired combination and distribution of pores. That is why alternative techniques have been used to try to predict these characteristics, such as physical models and the use of Computer Aided Design (CAD) [13]. CAD has allowed not only the generation of realistic models of metal foams, but also the characterization of their porous systems, even when these materials have fractal porosity. FEM is one of the methods used to model conventional and fractal foams, this due to its modeling capability for different geometries and pore arrangements [11, 13, 14]. Besides, using it is possible to determine characteristic parameters which define the foams, and to predict their mechanical properties. That is why in this work, as the first objective, we are using DEM-FEM models to replicate real metal foams with different fractal distributions of the porosity, to try to fill the gap related with this kind of materials. These generated foams presented different characteristic parameters, which were determined using image analysis, the tools of the FEA software (ANSYS), and tools proposed in this research, which search the optimum measurement method for each case. The influence of these parameters on the Young's moduli of such modeled fractal foams was also analyzed.

2. Modeling and simulation

2.1. Modelling fractal foams

As first part of this research, three fractal foams were modeled according to the presented in a previous work [13], using a combination of Discrete and Finite Element Methods. These models were designed combining particles (space holders) of different sizes and relative quantities between them, as shown in Figs. 1a)-1i). Particle sizes were 2 and 4 mm, while quantity ratio shows that the number of fine particles for each coarse particle in the mixture were 0, 2 and 4. According to these ratios, fractal distributions were 1 and 2, for the models of Figs. 1d)-1f) and 1g)-1i) [*log (relative quantities)/log (sizes ratio)*]. The model of Figure 1a-c represents a conventional foam, with simple porosity (no fractal). The process for obtaining foams with different porosities, including the fractal foams, consisted on first select the relative ratios, followed by the generation of a considerable amount of Representative Volume Elements (RVE), which is the minimum unit cell representing the complete foam [Figs. 1d) and 1g)]. In the models of packed spheres of Figs. 1b), 1e) and 1h), 10 RVE were initially used. It has been reported that RVEs must be at least $\sim$2.5$-$3.5 times the maximum size of certain feature that represents the material (unit cell) [15]. The size of the models will be modified, using different quantities of RVE, as will be further presented, in search of the convergence of both the porosity and the estimated mechanical properties. The packed spheres modeled here [Figs. 1b), 1e) and 1h)] represent the mixtures of the Space Holder Particles (SHPs) used for manufacturing conventional or fractal foams through techniques such as infiltration or powder metallurgy. Coordinates for the location of the SHPs were generated first through LIGGGTHS software [16]. This tool uses the Discrete Element Method for simulating the interaction between particles (in this case the SHPs mixing and packing processes), and generates spheres randomly distributed. To obtain the final models [see Figs. 1c), 1f) and 1i)], the DEM code was running up in the Design Modeler tool of the ANSYS FEM 19.0 software. Here, the solid spheres were subtracted to a solid cylinder with the desired dimensions (depending on the RVEs). These initial models have diameters and heights of 40 mm (10 times the diameter of the bigger pores, 4 mm).

Once the models were generated, different approaches were used to determine some characteristics and properties of the foams, studies which are presented next.

3. Results and discussion

3.1. Characteristics affecting porosity

3.1.1. Effect of the size of the RVE on porosity

As was commented above, the selection of a correct RVE is essential, because if the size is beyond a certain lower limit, the porosity is overestimated. This could redound in substantial errors in the determination of other properties, *e.g.* mechanical properties [17]. In our first analysis here, we are reducing the original size of the RVE to analyze the effect on the porosity. These calculations are for the model presented in Fig. 1a), which has pores of 4 mm and dimensions 10 times the size of the diameter of the pores. According to this, Fig. 2 shows the effect of the RVE size on the porosity, considering that this size is the ratio H/d, where H is the diameter of the model and d the size of the pores (4 mm). Starting from a desired porosity of 65.5 %, for the RVE with an original size of 10 porosity was 65.8 %. Then, the size of the RVE was reduced till reaching 2.5. As it can be seen, the size of the RVE significantly affected porosity. For RVE sizes higher than 3.5, porosities mismatched form 65.5 % only between $+0.6$ and -0.3 %, but for RVEs of 2.5 and 3.0 the deviations significantly increased. This result agrees with the previously reported about RVE higher than $\sim 2.5-3.5$ the size of the unit cell (pore) [15]. It is important to remark that the selection of the RVE not only includes its size but also its shape and other characteristics [18]. We are assuming values lower than 0.5 % as acceptable for their use in modelling, then, RVE higher than 5.5 are optima, and for our subsequent studies and the analysis of other properties, RVEs = 6 are used, not only for foams with only one pore size, but also for dual porosities. This convergence criterion was experimentally validated in a previous work, including a simplified hollow model where the representative volume element had at least four times the

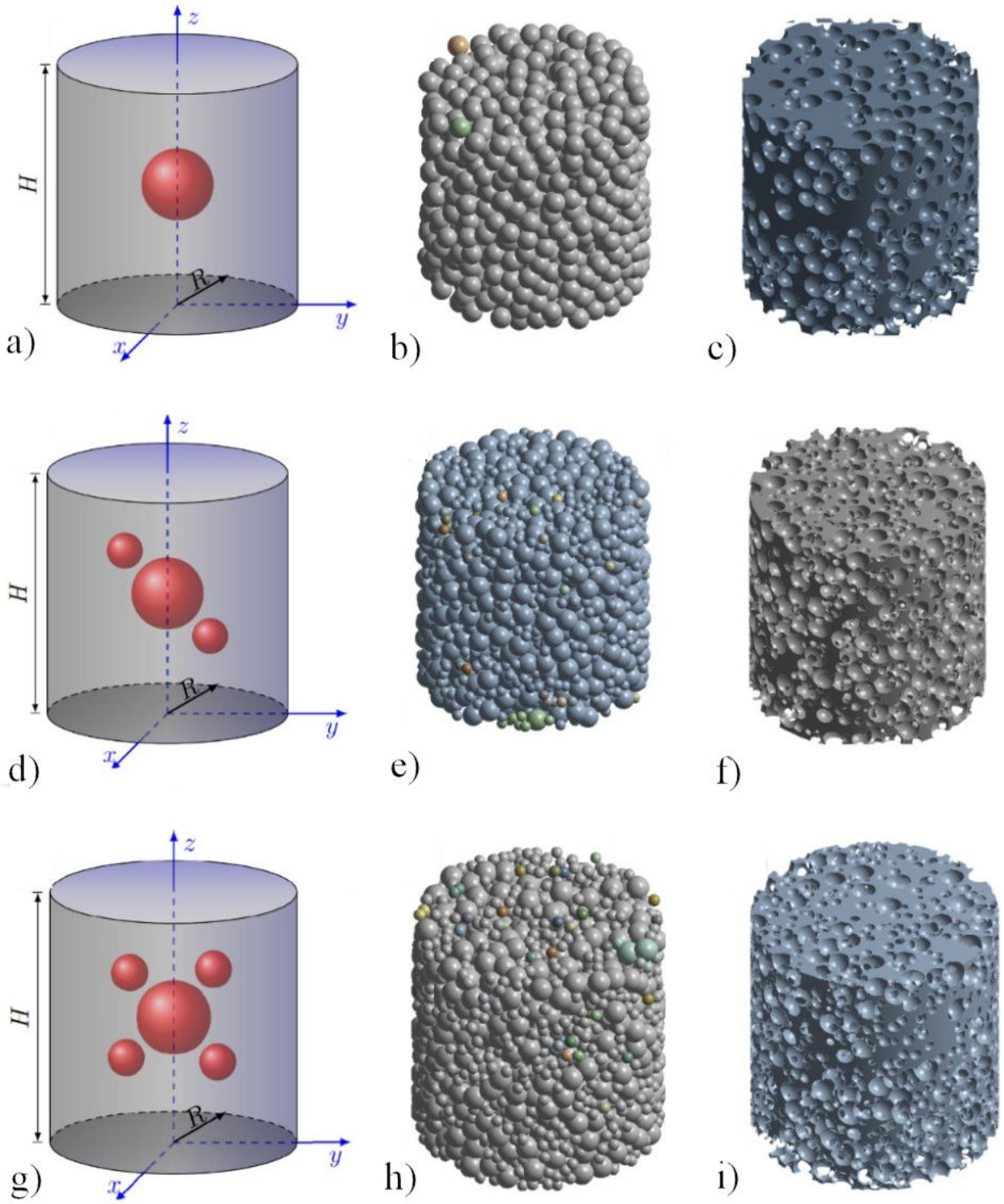

FIGURE 1. Isometric view of: a), d), g) different cylindrical unit cells with three quantity ratios, b), e), h) location of the space holders for the pores generation, and c), f), i) final fractal foam models.

size of a unit cell cite11. In models used for representing real foams, RVE must be thick enough to contain a significant quantity of unit cells.

According to the results above commented, we are presenting foams with RVEs = 6 in the subsequent analyses to decrease computational requirements. This can be seen in Fig. 3a)-3c) for RVEs with diameters and heights of 24 mm, porosities of 65% and the size ratios showed in Fig. 1. These models of the foams show homogeneous distribution of the pores, and are very similar to real foams found in literature

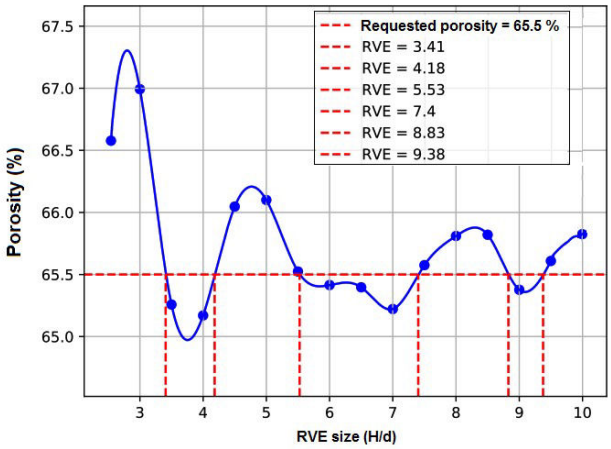

FIGURE 2. Effect of the RVE size on the obtained porosity in the foam models.

[4,7,11]. They are going to be the starting point for different analyses.

3.1.2. *Effect of the characterization method on the measured porosity*

The first analysis that we are including compares the measurement of the porosity of the foam models using different procedures. ANSYS has its own Javascript code tools for determining the solid and empty spaces in the generated geometries. Nevertheless, we are presenting a tool for comparing these measurements, verify and optimize the prediction of these porosities. This procedure uses Monte Carlo method through a Python code, and consists on selecting certain number of random points in the volume of the foam, and determine if they are located inside the solid matrix or in an empty space. Figure 4a)-4d) presents this method using from 5 000 to 30 000 points for a case of a porosity reduced to 26 %. The red points indicate pores, while the blue ones indicate matrix. Then, porosity is calculated as follows:

$$P = \frac{P_p}{P_m}, \tag{1}$$

where P_p and P_m are the points located inside pores and in the matrix, respectively. N points are evaluated, corresponding to N independent Bernoulli variables (X_j^n), being the function $f(X_j^n) = 1$ if a point is inside a pore, and zero in another case.

According to the observed in Figs. 4b)-d), the quantity of points is variable. Now, the effect of this number could significantly affect the porosity measurement. This is observed in Fig. 5a), where for less than 20 000 points the convergence does not occur yet. To compare the measurement times for ANSYS and for the procedure shown in Fig. 4, in Fig. 5b) presents the time used in each case depending on the number of pores of a foam. As can be seen, the method presented for our research groups is considerably lower. Time for ANSYS is exponential, while Monte Carlo is linear. Saved time for a geometry with 100 pores is 84 %, while for a geometry with 40 000 pores is 99 % less. It is important to remark the scale used in the Y axis. The long time used by ANSYS is because the Javascript code needs to be loaded in the ANSYS Design Modeler, but first executes the geometric operations to generate the foam before starting calculations.

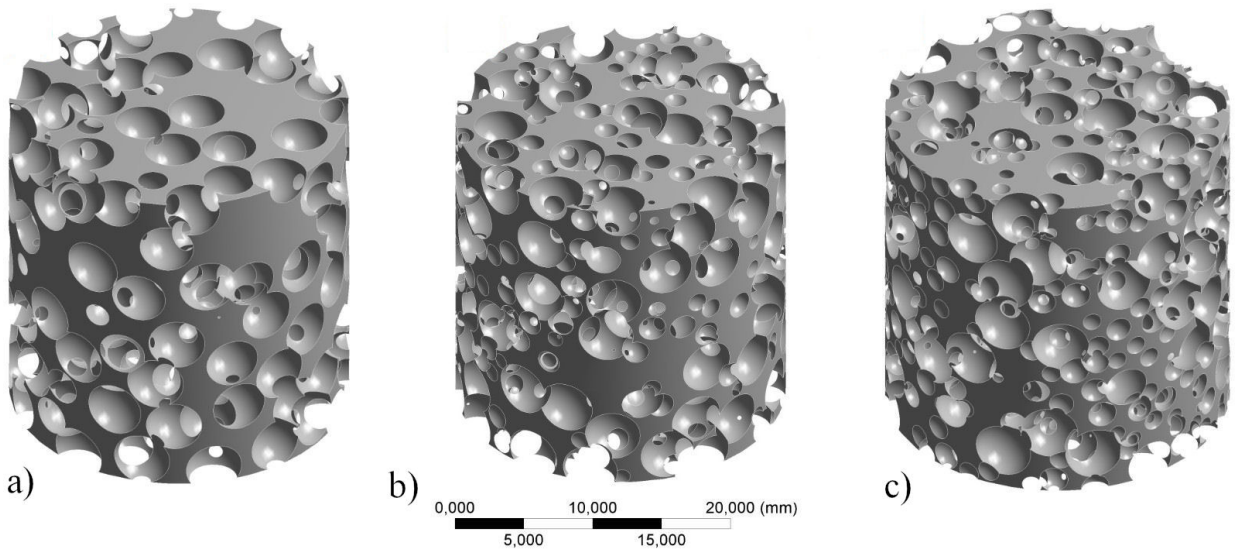

FIGURE 3. Models of foams with RVE = 6 and porosities of 65 % for: a) pores of a unique size, and pores with fractal morphologies of b) 2:1, and c) 4:1.

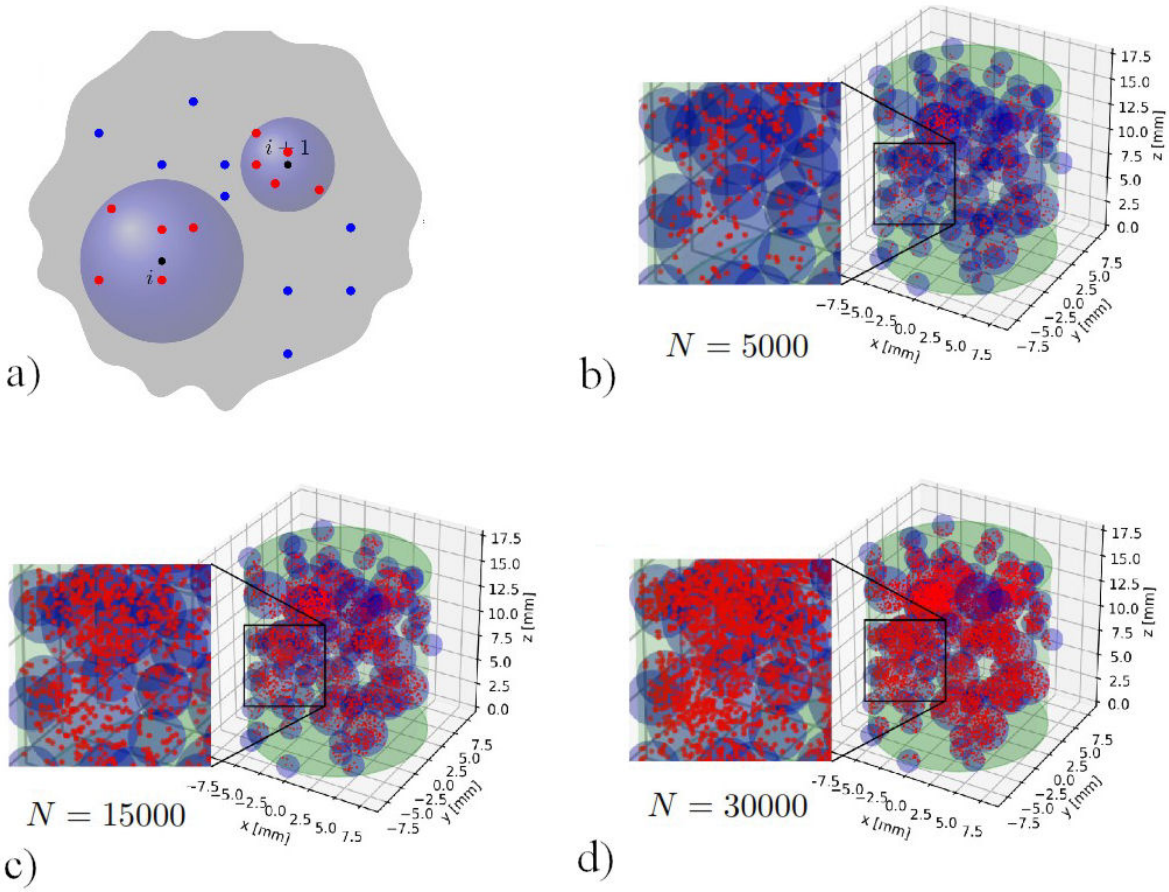

FIGURE 4. Identification of points for porosity control using Monte Carlo method through a Python code a), for N points: b) 5 000, c) 15 000, and d) 30 000.

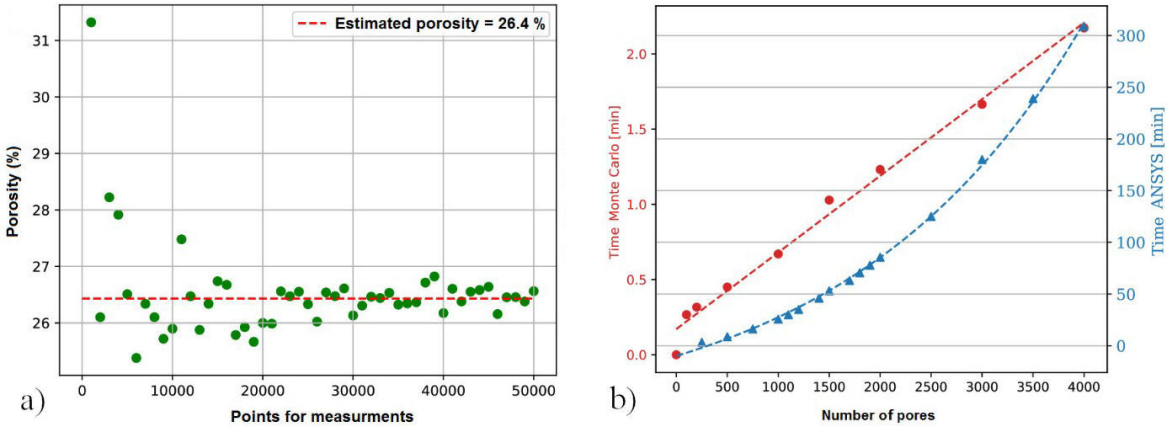

FIGURE 5. a) Convergence of the porosity for an increasing quantity of points used by the Monte Carlo method. b) Comparative time using Monte Carlo method or loading the Javascript code in the ANSYS Design Modeler.

3.1.3. Effect of the interconnectivity of the pores

Interconnectivity between the pores is another important parameter which affects the porosity of the foams and hence their mechanical properties. We are proposing here a new tool for completing this measurement, because ANSYS does not show these values. The procedure is observed in Fig. 6a), and consists on determining if each individual pore is interconnected with some of its neighbors. If the distance between the centers of the neighbor spheres (pores) is lower than the sum of the radius of these pores, then they are interconnected (green lines). Conversely, if this measurement is higher (red lines) they are isolated. This process is repeated until the analysis of all the pores. As can be seen in Fig. 6a), green

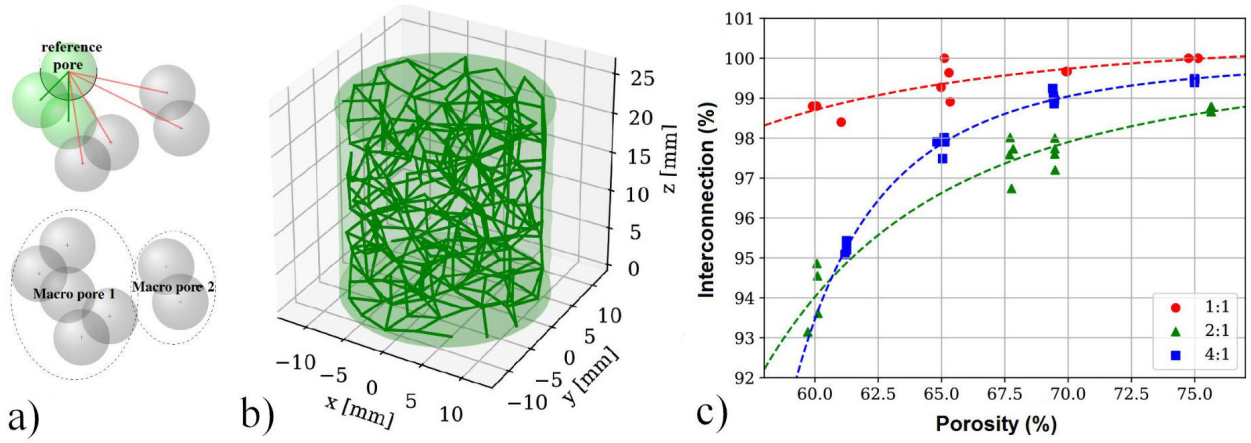

FIGURE 6. a) Measurement of the interconnection of pores through their neighbors, b) Network of lines belonging to interconnected pores, and c) Interconnection percentage according to the total porosity for different fractal models of foams.

pores form a macropore, and then they are interconnected (macropores 1 and 2). According to this, global interconnection (I) is measured through the following equation:

$$I = \frac{VP_I}{V_f}, \tag{2}$$

where VP_I is the volume occupied by the interconnected pores and V_f is the total volume of the foam. Figure 6b) shows an example of the interconnection of the pores through the green lines network belonging to macropores (pores interconnected in Fig. 6a). This procedure was used to determine the interconnection between the pores for different fractal models, as the presented in Figs. 1a)-1i), but with different porosities and sizes of the RVE. The results are presented in Fig. 6c), and as expected, the increase in the total porosity of a foam leads to significant increases of the interconnection percentage. This increment is more relevant for the fractal models than for the models with only one pore size due to the present of small pore interconnecting the bigger ones. Interconnectivity also affects directly other parameters, *e.g.* the wall thickness of the cells, which decreases for high interconnectivity levels, as occurs for foams manufactured by infiltration using SHPs previously sintered for obtaining green preforms [20]. In this process, the subsequent elimination of the SHP leads to obtain open cell foams (complete interconnection). By the contrary, in syntactic foams pores are not connected, being closed cells [21]. Due to the importance of the wall thickness on the mechanical properties, this characteristic of the foams is analyzed next. These results agree well with the experimental results of the work by Carranza *et al*. [14], who used similar models to compare their behavior with experimentally manufactured aluminum foams, and reported that when the relative quantities of pores increase from 1:1 to 4:1, wall thicknesses and densities significantly decreased, also leading to the increase of the interconnectivity, as it is observed in Fig. 6c).

3.1.4. Effect of the pore wall thickness on the porosity

Wall thickness could be defined as the distance W_n between two neighbor pores, as observed in Fig. 7a). This variable generally decreases with the increase in the total porosity of a foam, but also decreases with the inclusion of dual pores [20, 21]. Its measurement is needed for relating the pore network with the mechanical properties of the foams, and we are proposing here a procedure for its determination. It consists

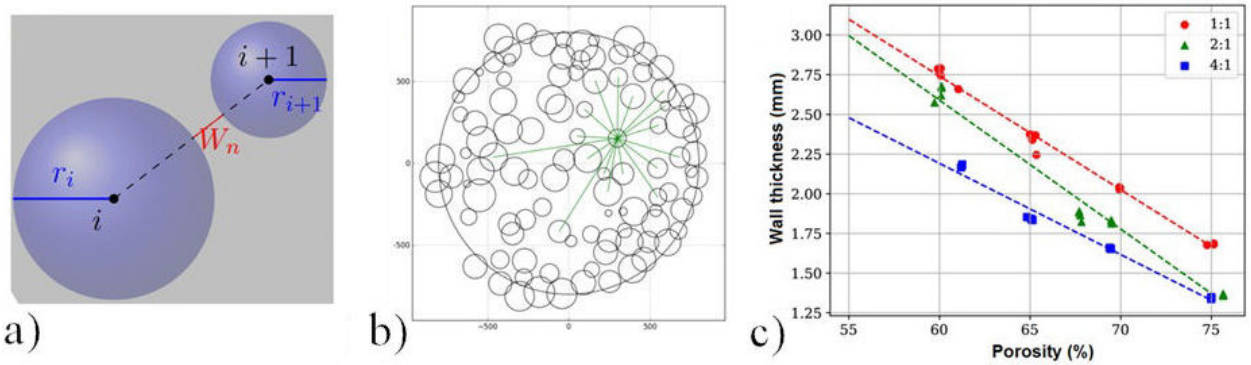

FIGURE 7. a) Cell wall thickness of neighbor pores (W_n), b) Measurement of the wall thickness for a pore, and c) Wall thickness obtained for different fractal models of foams.

on determining the distance W_n between a pore and all its neighbors, as shows Fig. 7b) with lines coming out of an individual pore (circle). If one of these lines past through the space between 2 pores is not considered for the average. This procedure was used to determine the wall thickness for pores of different fractal models with different porosities and sizes of the RVE, as the presented in Figs. 1a)-1i). The results are shown in Fig. 7c), and as expected, the increase in the total porosity of a foam leads to significant decrement in the wall thickness. Comparing the foam models, the increment is more relevant for the fractal models than for the models with only one pore size. This result can be explained since for fractal foams the wall thickness left by big pores is filled with small pores, reducing the solid part between the pores. This result also agrees with the experimental analysis carried out by Carranza *et al*. [19], who reported the same pore sizes (2 and 4 mm) for aluminum foams manufactured using infiltration. For porosities ranging from 63 to 66 %, they obtained wall thicknesses between 2 and 1.24 mm. Using our models, Fig. 7c) reveals wall thicknesses decreasing from 2.2 to 1.5 mm. Although these values are higher than the reported [19], this overestimation would be caused by some pore agglomerations in the models. Other work of Carranza *et al*. [14] demonstrated that depending on the manufacturing process (*i.e.*, infiltration or powder metallurgy), wall thickness is different, being near 2.3 mm for infiltration and a porosity of 65%.

3.2. Factors affecting mechanical properties estimation

3.2.1. *Effect of the mesh on the mechanical properties: convergence*

Once all the above characteristics of the models have been studied, it is the moment to analyze their simulation to estimate the mechanical behavior of the foams, and the influence of these characteristics on the porosity. For its determination, the response to the compression along the z-axis (E_z) was determined for the cylindrical models, applying equivalent compressive displacements of 1 % of the cylinder height on the nodes of the upper end of the cylindrical specimens. Besides, the coupled-node boundary condition was used for this face, while the bottom face was kept without movement. E_z is defined as follows:

$$E_z = \frac{\sigma_z}{\epsilon_z}, \tag{3}$$

where σ_z and ϵ_z are respectively the stress and strain in z-axis. The strain was determined through the applied displacement of the cylinder in the z-axis (u_z):

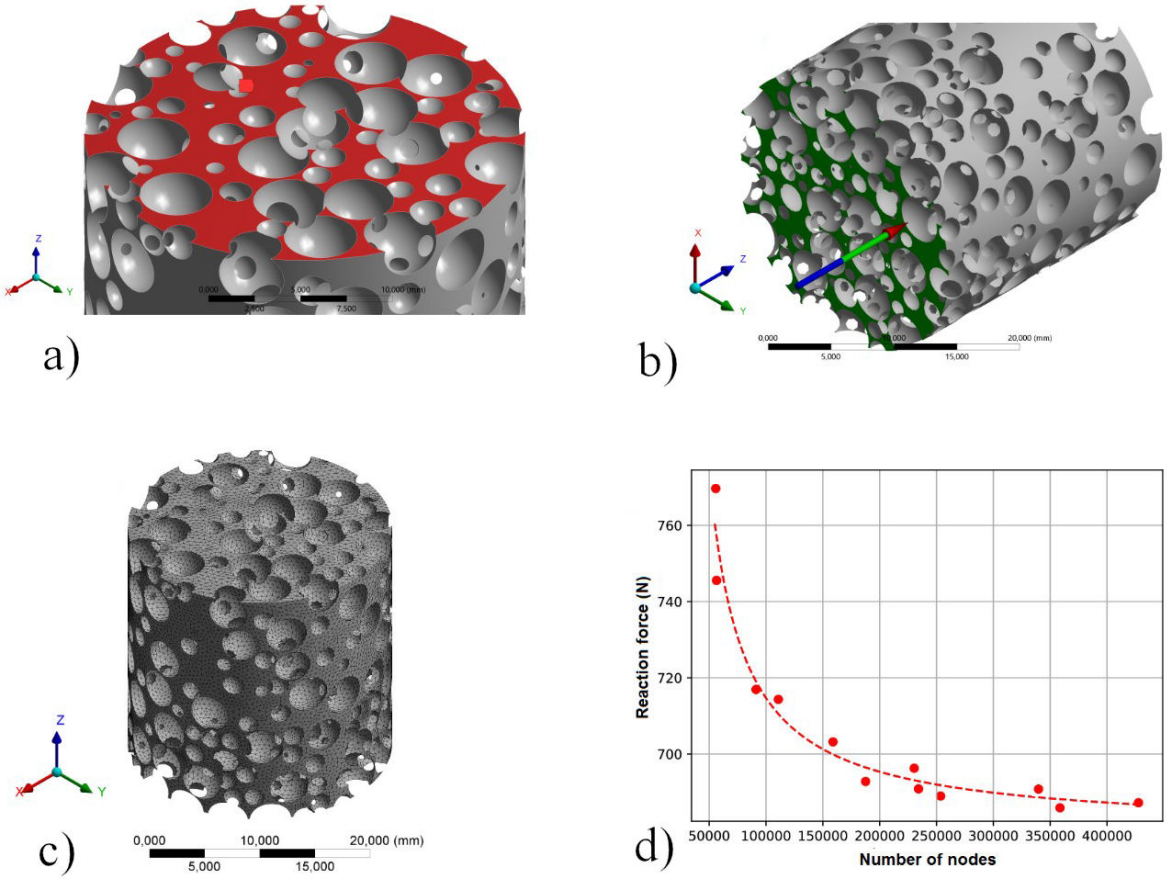

FIGURE 8. a) Top surface of a foam model, remarking the solid area. b) Reaction force on the bottom area of a foam model. c) FEA model of a foam with a porosity of 60 % and fractal distribution of 2:1. d) Effect of the number of nodes on the reaction forces.

$$\epsilon_z = \frac{u_z}{L_z}, \tag{4}$$

where L_z is the initial height of the cylindrical specimen. The stress, necessary for solving Eq. (3), is determined using the following equation:

$$\sigma_z = \frac{F_z}{A}, \tag{5}$$

where F_z is the reaction force in the z-axis obtained through the FEA simulation, for the nodes of the bottom end of the cylindrical specimens, which has an area A. According to this, the reaction force is the parameter to determine for obtaining the Young's modulus, and its value highly depends on the selected mesh. Figure 8a) shows the top surface of a foam model, while Fig. 8b) shows the illustration of the reaction force. In this work, we used 10-node tetrahedral structural solid elements for meshing. This can be observed in Fig. 8c) for a RVE with a porosity of 60 % and fractal distribution of 2:1, remarking the fine mesh. The selection of low number of nodes could lead to significant differences with the real behavior of the foam, while a fine mesh could originate too much computing time. Then, it is essential to analyze the limit number of nodes which leads to a plateau behavior of the reaction forces. This was studied in this work, and as can be seen in Fig. 8d), reaction forces begin to converge approximately after 250 000 nodes. Then, this number of nodes was taken as the starting point for meshing in all subsequent simulations.

3.2.2. Effect of the pore network on the mechanical properties

Using the optima data obtained above, the mechanical behavior of the foam models is presented next. First, Fig. 9a) corroborates the effect of the RVE size not only on the porosity (see Fig. 2) but also on Young's modulus. The porosity decreased for small RVEs, and the same happened for the values of the relative modulus for both conventional and fractal foams, showing that for RVEs bigger than ~ 4 plateaus were reached (convergence). On the other hand, Fig. 9b) depicts the effect of the porosity on the relative Young's modulus. As can be seen, this variable decreases with the increase in the porosity of the foams, but no significant differences are observed depending on the fractal characteristics of the models. Contrary was the behavior of the wall thickness presented in Fig. 9c), where the increase in this dimension leads to higher values of the relative Young's modulus. The estimated relative Young's moduli of Fig. 9c) agree with the experimentally obtained for similar foams in the work of Carranza *et al*. [14], this for an aluminum foam. They reported Young's modulus of 1.52, 1.12, and 0.51 MPa for pore relative quantities of 1:1, 2:1, and 4:1, with wall thicknesses of 2, 1.63, and 1.24, respectively. According to Fig. 9c), relative Young's modulus for these similar conditions are 0.08, 0.07, and 0.04, corresponding to Young's modulus of 5.6, 4.9, and 2.8 GPa. Although these values are overestimated, it is an expected result due to the above-mentioned problems with the pore agglomeration, but the tendency is like the experimental foams, which demonstrated the efficiency of our models for comparative purposes. Results also show that the inclusion of a higher quantity of small pores for fractal models led to higher relative moduli. These behaviors could be explained according to the observed in Figs. 6c) and 7c), where for the same porosity the inclusion of dual pores decreased the interconnection percentage (Fig. 6c), but also led to decrease the wall thickness (Fig. 7c). It is well known that Young's modulus decreases for high porosities and interconnectivities, and for small wall thicknesses, which agree with the results obtained here. Nevertheless, the combination of these variables needs to be analyzed together, because each of them affects mechanical properties. That is why the fractal dimension (D_f) was used as comparative parameter, unifying in only one variable the possible combined effect of the porosity, the interconnectivity and the wall thickness. This is shown in Fig. 9d), where for the same fractal dimension the relative moduli are always higher for the conventional foams models, followed by fractal models 2:1 and 4:1. Besides, the increase in the fractal dimension leads to the increase in the relative modulus. It is important to remark how the fractal dimension was determined here, and to remember that this variable is a measure of the complexity of an image. In previous works D_f was introduced, including its measurement using 2D images of foams through the box-counting method [20, 21]. Due to the importance of the solid matrixes, D_f was obtained from their analysis (solid part of the foams). This is observed in Fig. 9e) for model 1:1, 2:1 and 4:1, where the complexity of the images varies for the black part, decreasing D_f for the white matrix. To corroborate this effect, Figs. 9f) and 9g) depict the behaviors of D_f depending on the porosity and the wall thickness. Fractal dimensions were always higher for the fractal foams than for the conventional ones. Besides, low porosities and big wall thicknesses led to high values of D_f. This demonstrates the importance of D_f for the analysis of the pore network and its effect on the mechanical properties above analyzed.

As was observed in Figs. 9b) to 9d), the most important parameter for estimating the Young's modulus was the porosity volume fraction. This was demonstrated in Fig. 9b), where curves did not present significant differences, and only changes in porosity modified the Young's moduli, without influencing pore sizes. That is why almost all the reported models for estimating Young's modulus are based on porosities or densities of the foams. Four of these models were used to compare the effectiveness of our FEA estimations: Gibson and Ashby [22], Zhu et al. [23], Warren and Kraynik [24], and Nielsen [25]. These approaches use relative densities as the variable to be considered. Estimation using these models and our FEA results [see Fig. 9b)] can be seen in Table I for estimations based on aluminum foams with porosities of 60, 65 and 70 % (for Al, $E = 70$ GPa, $\rho = 2.7$ g·cm^{-3}). Compared to our FEA estimations, Nielsen's model results are significantly higher; while Zhu, and Warren and Kraynik's models under-estimated the Young's modulus. In contrast,

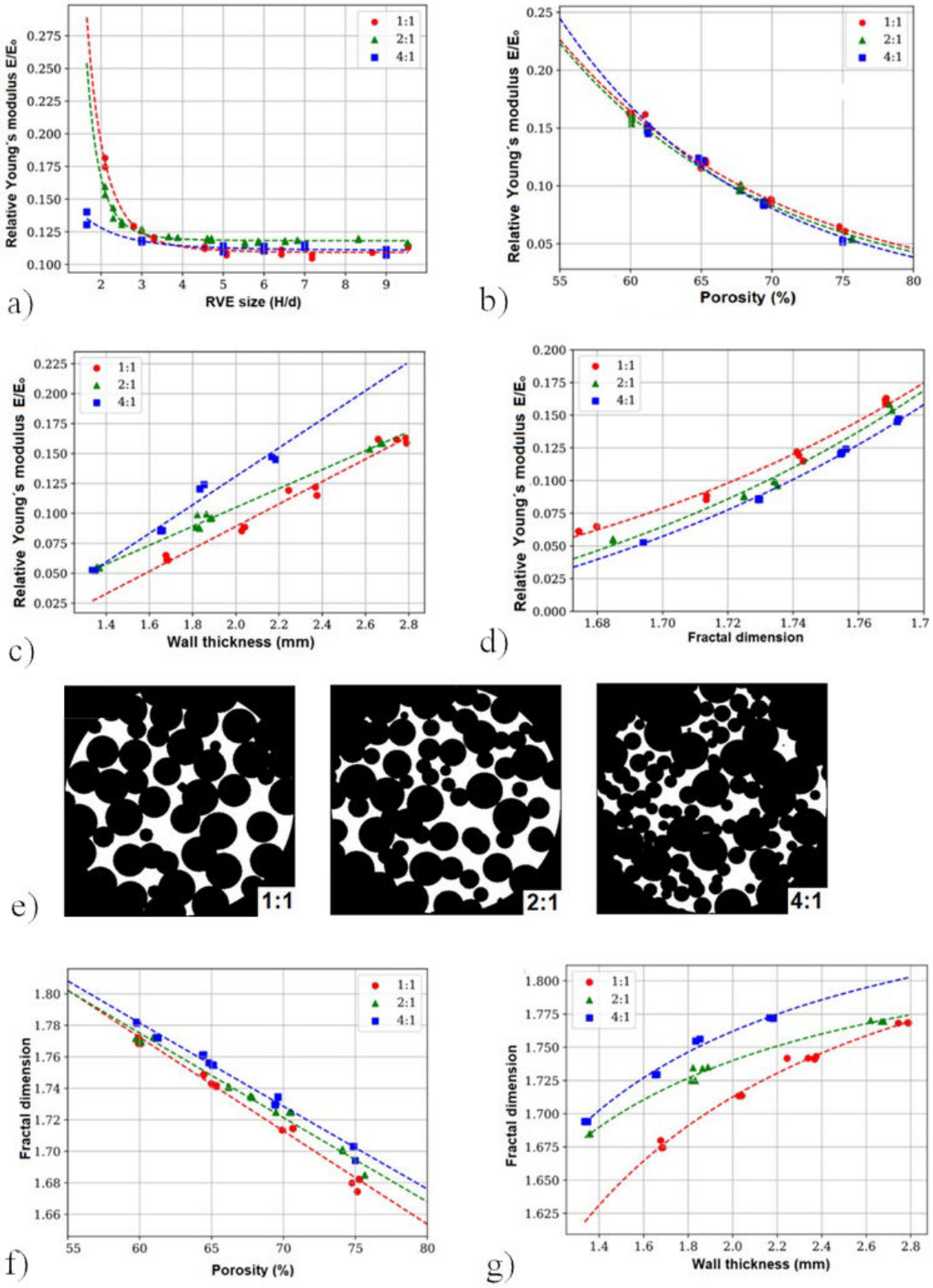

FIGURE 9. Effect on the relative Young's modulus of: a) RVE size b) porosity, c) wall thickness, and d) fractal dimension. e) Cross section for the models of conventional and fractal foams. Behavior of the fractal dimension depending on the porosity f) and the wall thickness g).

TABLE I. Relative Young's modulus of theoretical models and simulation.

Model	Porosity (%)		
	60	65	70
Ansys simulation	0.16 ± 0.02	0.12 ± 0.01	0.09 ± 0.02
Zhu	0.10 ± 0.01	0.08 ± 0.01	0.06 ± 0.01
Warren-Kraynik	0.09 ± 0.01	0.07 ± 0.01	0.06 ± 0.01
Nielsen	0.36 ± 0.05	0.31 ± 0.04	0.27 ± 0.04
Gibson-Ashby	0.15 ± 0.02	0.13 ± 0.02	0.11 ± 0.01

the results obtained by the Gibson-Ashby model are very close to the predictions obtained by our FEA models. Except for FEA and Gibson-Ashby models, all the other mathematical estimations only use the porosity percentage and not their distribution, being generally far from real experimental values.

4. Conclusions

In this work, conventional and fractal models of foams were generated combining FEM and DEM. Pore network characteristics of such models were analyzed using different measurement methods, focusing on the porosity percentage, the convergence of the results depending on the size of the Representative Volume Element, the interconnectivity of the pores, the wall thickness, and the fractal dimension. It was concluded that for the convergence of the porosity and the estimation of the mechanical properties, the size of the RVE needs to be higher than ~ 4 to 5 times the size of a unit cell which represents the whole foam. Besides, a procedure using Monte Carlo method through a Python code was introduced and used to successfully determine the porosity percentage and the above commented characteristics. Besides, the fractal dimension demonstrated to be an excellent tool for combining the effect of the complexity of the pore network on the mechanical properties.

Acknowledgments

Authors acknowledge the financial support from UNAM-PAPIIT IN102322 project.

1. F. García-Moreno, Commercial applications of metal foams: Their properties and production, *Materials* **9** (2016) 85, https://doi.org/10.3390/ma9020085
2. T. Wan, Y. Liu, C. Zhou, X. Chen, Y. Li, Fabrication, properties, and applications of open-cell aluminum foams: A review, *J. Mater. Sci. Technol.* **62** (2021) 11, https://doi.org/10.1016/j.jmst.2020.05.039
3. C. Kádár, P. Kubelka, A. Szlancsik. On the compressive properties of aluminum and magnesium syntactic foams: Experiment and simulation, *Mater. Today Comm.* **35** (2023) 106060, https://doi.org/10.1016/j.mtcomm.2023.106060
4. J. Banhart, Manufacture, characterization and application of cellular metals and metal foams, *Prog. Mater. Sci.* **46** (2001) 559, https://doi.org/10.1016/S0079-6425(00)00002-5
5. P. Colombo, D.C. Dunand, V. Kumar, Porous materials: Less is more, *J. Mater. Res.* **28** (2013) 2187, https://doi.org/10.1557/jmr.2013.232
6. X.Y. Yang, L.H. Li, Y. Li, J.C. Rooke, C. Sanchez, and B.L. Su, Hierarchically porous materials: synthesis strategies and structure design, *Chem. Soc. Rev.* **46** (2017) 481, https://doi.org/10.1039/c6cs00829a
7. B.Y. Casas, J.C. Carranza, L. Béjar, C. Aguilar, I.A. Figueroa, and I. Alfonso, Production of aluminum foams with hierarchical porosity by a combination of two different manufacturing methods. *J. Alloy Compd.* **831** (2020) 154780, https://doi.org/10.1016/j.jallcom.2020.154780
8. A. Hassan, I.A. Alnaser, A review of different manufacturing methods of metallic foams, *ACS Omega* **9** (2024) 6280, https://doi.org/10.1021/acsomega.3c08613
9. A. Kulshreshtha, S.K. Dhakad, Preparation of metal foam by different methods: *A review, Mater. Today-Proc.* **26** (2020) 1784, https://doi.org/10.1016/j.matpr.2020.02.375
10. A. Nawaz, S. Rani, Fabrication methods and property analysis of metal foams - a technical overview, *Mater. Sci. Tech.* **39** (2023) 1877, https://doi.org/10.1080/02670836.2023.2186068
11. L. Pérez, S. Lascano, C. Aguilar, D. Domancic, I. Alfonso, Simplified fractal FEA model for the estimation of the Young's modulus of Ti foams obtained by powder metallurgy, *Mater. Design* **83** (2015) 276, https://doi.org/10.1016/j.matdes.2015.06.038
12. N. Behymer, K. Morsi, Review: Closed-cell metallic foams produced via powder metallurgy, *Metals* **13** (2023) 959, https://doi.org/10.3390/met13050959
13. C Reyes, L. Béjar, J.C. Carranza, P. Pérez, L. Pérez, I. Alfonso, DEM-FEM combination for modelling and simulation of fractal metallic foams, *Mater. Today Comm.* **34** (2023) 105054, https://doi.org/10.1016/j.mtcomm.2022.105054
14. J. C. Carranza, L. Pérez, R. Ganesan, B.Y. Casas, R.A.L. Drew, C. Ruiz-Aguilar, I.A. Figueroa, I. Alfonso, Effect of fractal distribution of the porosity on mechanical properties of Al foams manufactured by infiltration, *J. Braz. Soc. Mech. Sci.* **41** (2019) 379, https://doi.org/10.1007/s40430-019-1876-7

15. S.K. Sebsadji, K. Chouicha, Determining periodic representative volumes of concrete mixtures based on the fractal analysis, *Int. J. Solids Struct.* **49** (2012) 2941, https://doi.org/10.1016/j.ijsolstr.2012.05.017

16. C. Kloss, C. Goniva, A. Hager, S. Amberger, S. Pirker. Models, algorithms and validation for opensource DEM and CFD-DEM. *Prog. Comput. Fluid Dyn.* **12** (2012) 140, https://doi.org/10.2298/TAM210129005R

17. Y. Hu, Q. Fang, J. Qian, Effect of cell structure on the uniaxial compression properties of closed-cell foam materials, *Mater. Today Comm.* **26** (2021) 102104, https://doi.org/10.1016/j.mtcomm.2021.102104

18. C. Grill, S. Diebels, A. Jung, Determination of an RVE and identifying a representative idealised model for specific surface and volume of metal foams, *Mater. Today Comm.* **38** (2024) 108317, https://doi.org/10.1016/j.mtcomm.2024.108317

19. J.C. Carranza, B.Y. Casas, I. Alfonso, L. Pérez, R.A.L. Drew, J.A. Verduzco, I.A. Figueroa. Estimation of the pores agglomeration effect on the compressive behavior of metallic foams: infiltration and powder metallurgy study cases, *J. Theor. Appl. Mech.* **50** (2020) 176, https://doi.org/10.7546/JTAM.50.20.02.07

20. R. Thiyagarajan, M. Senthil Kumar, A review on closed cell metal matrix syntactic foams: A green initiative towards eco-sustainability, *Mater. Manuf. Process.* **36** (2021) 1333, https://doi.org/10.1080/10426914.2021.1928696

21. C. Reyes, I. Alfonso, L. Béjar, L. Pérez, C. Aguilar, J.C. Carranza, L.E. Carranza, Use of the fractal dimension for porosity modification in aluminum foams manufactured using space holder particles, *Theor. Appl. Mech.* **48** (2021) 109, https://doi.org/10.2298/TAM210129005R

22. M. Ashby, The properties of foams and lattices, *Philos. Trans. R. Soc. A Math. Phys. Eng. Sci.* **364** (2005) 15, https://doi.org/10.1098/rsta.2005.1678

23. H.X. Zhu, N.J. Mills, J.F. Knott, Analysis of the high strain compression of open cell foams, *J. Mech. Phys. Solids* **45** (1997) 1875, https://dx.doi.org/10.1016/S0022-5096(97)00027-6

24. W.E. Warren, A.M. Kraynik, The linear elastic properties of open cell foams, *J. Appl. Mech.* **55** (1988) 341, https://dx.doi.org/10.1115/1.3173680

25. L.F. Nielsen, Elasticity and damping of porous materials and impregnated materials, *J. Am. Ceram. Soc.* **67** (1984) 93, https://dx.doi.org/10.1111/j.1151-2916.1984.tb09622.x